A MECHANISTIC FORCE MODEL FOR SIMULATING HAPTICS OF HAND-HELD BONE BURRING OPERATIONS

A Thesis

by

AVINASH DANDA

Submitted to the Office of Graduate and Professional Studies of
Texas A&M University
in partial fulfillment of the requirements for the degree of

MASTER OF SCIENCE

Chair of Committee,	Bruce Tai
Co-Chair of Committee,	Mathew Kuttolamadom
Committee Members,	Jyhwen Wang
Head of Department,	Andreas Polycarpou

August 2017

Major Subject: Mechanical Engineering

ABSTRACT

The research presented in the thesis is concentrated on developing a mechanistic model to predict the forces experienced during bone burring with application to haptic feedback for virtual reality surgical simulations. This model can be used in haptic devices to provide haptic feedback for virtual reality (VR) surgical simulations. The model is developed based on the understanding of the force profile recorded in the experiments. To determine the force produced under various cutting orientations, experiments are conducted using a surgical burr on a synthetic bone. The total force experienced in bone burring can be understood as a combination of resistive force and vibrational force. The resistive force is calculated using the concept of the specific cutting energy of the bone material. The specific cutting energy (U_s) is a concept adopted from the mechanics of grinding. Data from the experiments is used to calibrate the specific cutting energy of the material. The vibrational force is developed as an empirical component of the coupled model. Comparisons between the experimentally measured force data and the force profile predicted by the model show a similar trend. Results confirm that the proposed model is capable of effectively predicting the haptics in bone burring, specifically with the abrasive type of burr.

ACKNOWLEDGEMENTS

I would like to thank the committee chair, Dr. Bruce Tai, co-chair, Dr. Mathew Kuttolamadom, and committee member Dr. Jyhwen Wang for their guidance and support throughout the process of this research.

I would also like to thank the funding support from the AggiE_Challenge program of Texas A&M University, and the participation of students enrolled in ENGR 491-519 (Fall 2015, Spring 2016).

Finally, thanks to my friends and colleagues and the department faculty and staff for making my time at Texas A&M University a great experience.

CONTRIBUTORS AND FUNDING SOURCES

This work was supervised by a thesis committee consisting of the committee chair, Dr. Bruce Tai [MEEN], co-chair, Dr. Mathew Kuttolamadom[ETID], and committee member Dr. Jyhwen Wang [ETID].

All work for the thesis was completed by the student, under the advisement of Dr. Bruce Tai [MEEN] and Dr. Mathew Kuttolamadom[ETID]. Dr. Vinayak [MEEN], and Dr. Harry Hogan [MEEN], attended the thesis defense and provided valuable feedback for the future work.

This work was made possible in part by the funding from the AggiE-Challenge program, Texas A&M University.

NOMENCLATURE

$\overrightarrow{F_r}$	Resistive force
$\overrightarrow{F_v}$	Vibrational force
$\overrightarrow{F}$	Total force
$\overrightarrow{F_t}$	Elemental tangential force
$\overrightarrow{F_n}$	Elemental normal force
V	Volume
U_S	Specific cutting energy
K	Constant normal to tangential force ratio
$\overrightarrow{F}_{feed}$	Feed force
$\overrightarrow{F}_{lateral}$	Lateral force
$\overrightarrow{F}_{normal}$	Normal force
$\overrightarrow{F_r}$	Resultant force
$\overrightarrow{F_g}$	Vibrational force in burring
$\overrightarrow{F_d}$	Vibrational force during non-burring
$\overrightarrow{F_{vx}}$	Vibrational force recorded along x-axis of the dynamometer
$\overrightarrow{F_{vy}}$	Vibrational force recorded along y-axis of the dynamometer
$\overrightarrow{F_{vz}}$	Vibrational force recorded along z-axis of the dynamometer
$\overrightarrow{f}$	Unit vector in feed direction

$\vec{l}$	Unit vector in lateral direction
$\vec{n}$	Unit vector in normal direction
$\overrightarrow{v_f}$	Feed rate
$\vec{A}$	Elemental Area vector

TABLE OF CONTENTS

Page

LIST OF FIGURES

Page

LIST OF TABLES

Page

CHAPTER I

INTRODUCTION AND LITERATURE REVIEW

1.1 Motivation

Haptic devices incorporated with virtual reality (VR) systems are increasingly being used in medical training to simulate surgeries. Haptic devices use algorithms based on a force model to calculate forces produced during manipulation of soft and hard tissues. However, creating realistic haptic feedback could be challenging for operations involving biological material removal or fracture, such as bone machining and needle insertion, because of the highly dynamic and non-linear responses as opposed to simple contact and deformation models. Therefore, there is a need for an effective mathematical model to compute this force feedback that can be used by the haptic device.

1.2 Existing models for calculating force feedback

Several haptic force models are developed in the last decade to simulate bone tissue removal, especially dental and temporal bone surgery. Many of them are not physics-based, i.e., they do not consider the underlying physical phenomena during bone machining. We can broadly classify the work done in force modeling into physics based and non-physics based models.

1.2.1 Non-physics based models for calculating force

Non physics based models typically do not provide a relation between the forces and the mechanical properties of the bone. Also, the mechanisms such as chip formation

and plastic deformation are not taken into account in any of these models. The outputs generated by these models are tuned to match the experimental results so the final model will generate more realistic results. Most of the models used in the non-physics based category use penalty based techniques.

Wiet et al. [1] developed haptic algorithm that simulates a virtual "force-field" surrounding the virtual burr. They achieved the force-field by a set of virtual springs that uniformly distributed around the virtual burr, and a haptic algorithm that assigns each spring a stiffness and rest length. Petersik et al. [2] presented a haptic rendering algorithm for temporal bone cutting processes based on a ray-casting algorithm (Fig. 1). The interaction forces are calculated based on collision between an arbitrary sized sphere-shaped tool and an arbitrary complex anatomic model. All surface points which are inside the volume are traced in direction of the inward pointing normal until sphere center point is reached. All vectors are added and the direction and magnitude of the resulting vector is the force vector feedback to the haptic device. The results were finally scaled to the experimental results.

Wang et al. [3] used a Piecewise Contact Model based on interaction status transition. This model is proposed to describe the dynamic cutting process. They used a triangular mesh and a point-based unilateral spring force model to compute the virtual interaction force.

Kim and Park. [4] Introduced a single point of the virtual tool for force computation based on an offset surface in their haptic dental simulation system. Point based approaches do not take into consideration the parameters such as spindle speed and

tool geometry. Yoshida et al [5] constructed a multilayered tooth model into their virtual system, and through experiments a spring coefficient and a damping coefficient of a dental hard tissue were determined.

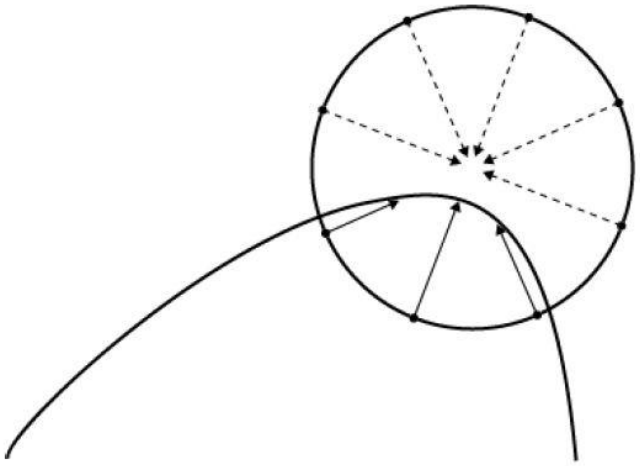

Figure 1. Implementation of ray tracing algorithm to calculate collision forces

Vibration is not taken into consideration in almost all of the techniques mentioned above. Usually these models are developed only to simulate forces on the haptic device. And the penalty based methods should always be tuned to emulate the experimental results to provide a most realistic simulation.

1.2.2 Physics based models for calculating force

Physics based models are the once that provide the relation between the forces and the mechanical properties of the bone. Several approaches that tend to correlate the forces generated during operation to the physical properties of a bone are followed by some researchers. The most common approaches are the once based on Hertz's contact theory, Impulse based dynamics and Specific cutting energy.

1.2.3 Physics model based on Hertz's contact theory

Agus et al. [6] assumed an elastic deformation between the rotating spherical tool and the bone and used Hertz's contact theory to determine the elastic force. The response forces at least within some limits are physically reasonable. But, the model still fails to provide a relation between the forces and mechanical properties of the bone. Moreover, any comparison with the experimental data still does not exist with this model.

1.2.4 Physics model based on specific cutting energy

Arbabtafti et al. [7-9] developed a physics based model for haptic simulation of bone machining. The physical principle behind the model is that the energy required to remove a unit volume of bone is a constant for a particular bone material. This principle is used to derive the forces required to remove bone material. The force of interaction between a cutting element and bone is calculated from the energy required to remove a bone chip with an estimated thickness and known material stiffness. Since the parameters such as bone material properties, tool geometry and spindle speed are used to compute forces for the haptic device, this is can be considered a physics based model. Fig. 2 gives an idea of how the model is built. One of the major drawback for the model is the computational cost which is a direct result of a complex modeling that is necessary for the simulation. Moreover, the model still doesn't account for the vibrations generated from the bone cutting.

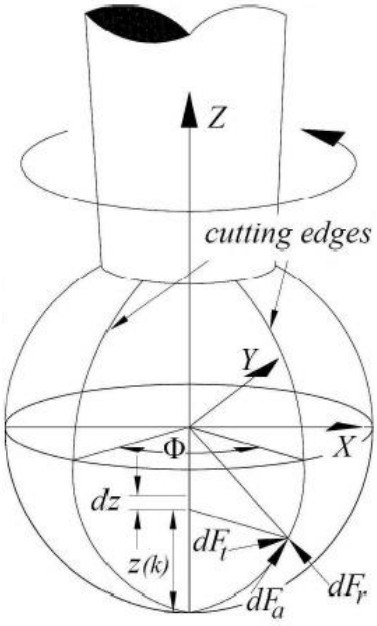

Figure 2. Image shows the forces acted on each point during the cutting process.

1.2.5 Physics model based on impulse based dynamics

Wang et al. [10] used impulse-based method to model haptics bone-burring interactions. The final model successfully correlated the physical properties of the bone to model the equations that derive force feedback. The use of this model achieved high computational efficiency and was also able to simulate various forces like resistance, friction and vibration. The model also calculated the vibration caused by the unbalanced contacts between the spherical burr and the bone.

However, the method cannot be classified as purely physics based. This is because the approach uses several assumptions to implement the “impulse” based techniques for the bone machining.

1.3 Models for calculating vibrations for enhancing haptics

Very few models used in haptics enhanced simulators implemented vibrations feedback. Okamura et al [11, 12] worked on creating a realistic vibro-tactile feedback for tasks like tapping on materials. They created a library of vibration signal parameters by experiments. Exponentially decaying sinusoid whose parameters depend on the material is used to model vibrations using experimental data. Vibrations selected from this library based on material properties are played back to the user through a haptic interface interacting with the virtual environments. Experiments involving human subjects were performed to validate their model. The results indicated the vibration feedback enhanced virtual environments.

Kuchenbecker et al [13] Implemented event-based haptics to enhance the reality of virtual objects. Contrary to the conventional methods in which a force-displacement relationship is used to model the feedback force, event-based haptics used pre-computed transients and display them open-loop. In this model the dynamic contact is viewed as superposition of two distinct forces. One is a high frequency transient force and the other is a low-frequency force that opposes penetration over long durations. This model used acceleration matching strategy to enhance reality.

Wang et al calculated the vibration caused by burring operation based on the approach proposed by Altintas et al. [14]. The forces are used to calculate the vibration displacement using a transfer function. This vibration displacement is used to calculate the vibration force which is finally added to the contact force and transmitted to the haptic device.

1.4 Human perception of vibration

Understanding the human perception is important consideration in designing the haptic feedback. This understanding will help us make assumptions in the modeling that will enhance the realism of a simulation. For example, it is well known from the literature that humans cannot sense the direction of high frequency low amplitude vibrations felt by the skin receptors [15]. This implies that the vibration generated by the haptic device can be in any direction to provide a realistic feedback as long as it is high frequency and low amplitude. Moreover, the devices designed based on the model presented can also be optimized without sacrificing the target realism of the simulation

Force, Pressure, Vibration and Stiffness perception are some of the factors to be considered for design of a haptic device. The force display resolution should match the human sensing resolution for the subject to perceive the forces as smoothly varying. A lot of research has already been done to determine the range and resolution of these factors.

Durlach et al [16] published a set of papers in which he dealt with the manual discrimination of force, compliance and physical characteristics such as length by human subjects using a simple electro mechanical device. The Just noticeable Difference (JND) for the force perception from these papers is found to be 7% on an average regardless of test conditions. Bolanowski et al [17] presented that the detection threshold of vibrotactile stimulation is 28 dB (re 1 micron) below 30 Hz and decreases at a rate of roughly -12 dB/oct from 30 to 300 Hz.

In addition to most of the above factors, Mandayam et al [18] presented results of position sensing resolution, pressure perception resolution and stiffness resolution using

his experiments. They presented an experimental setup to determine the minimum stiffness value required to simulate a rigid body. Several joints such as PIP, MCP, wrist (flex and extend), elbow (flex and extend), and shoulder were individually activated in separate trials and tested for the minimum stiffness value required to simulate a rigid body. The resultant values varied from 153 to 415 Newton/cm with the average being 242 Newton/cm. The joint angle resolution for wrist, elbow and shoulder are found to be 2.0°, 2.0° and 0.8° respectively

CHAPTER II

EXPERIMENTS

A concrete understanding of how cutting parameters effect forces and vibrations in bone grinding is necessary to develop a mechanistic model. This can be partly achieved by designing experiments to find the effects of various cutting parameters on the forces and vibrations produced in bone grinding. These experiments will also help us in calibrating the specific cutting energy values of the material, a value that will be used in developing the force model.

2.1 Experimental setup

The experimental setup is designed to explore the effects of orientation and cutting angle on the forces and vibrations produced during bone burring. This can be achieved by recording the force profiles produced when burring a synthetic cortical bone using a surgical drill at different orientations. The synthetic cortical bone is made using 3D printer ProJet® 160 and hardened with epoxy, by following a composition-recipe to mimic the properties of real human bone. This synthetic bone can better simulate a burring process on the cortical bone compared to the currently available commercial products [19, 20]. The setup for the experiments is shown in Fig. 3. The workpiece (synthetic bone) is attached to a powered linear slider. The linear slider will provide the constant velocity needed to control the feed rate during the experiments. The surgical tool (Stryker TPS 5100-50 Irrigation Console, MI, USA) is attached to the dynamometer (Kistler Model

Type 9272, NY, USA) using a customized fixture, and the dynamometer is placed on a manual slider. Several fixtures were 3D-printed to simulate different burring orientations. The surgical tool was held stationary and the workpiece moved along the length of the linear slider with a constant velocity (feed rate). The dynamometer is connected to a data acquisition system that samples the force in X, Y, and Z directions simultaneously at 3 kHz (the dynamometer's natural frequency is around 5 kHz.). The depth of cut can be manipulated by moving the dynamometer along the direction normal to the synthetic bone surface using the manual slider.

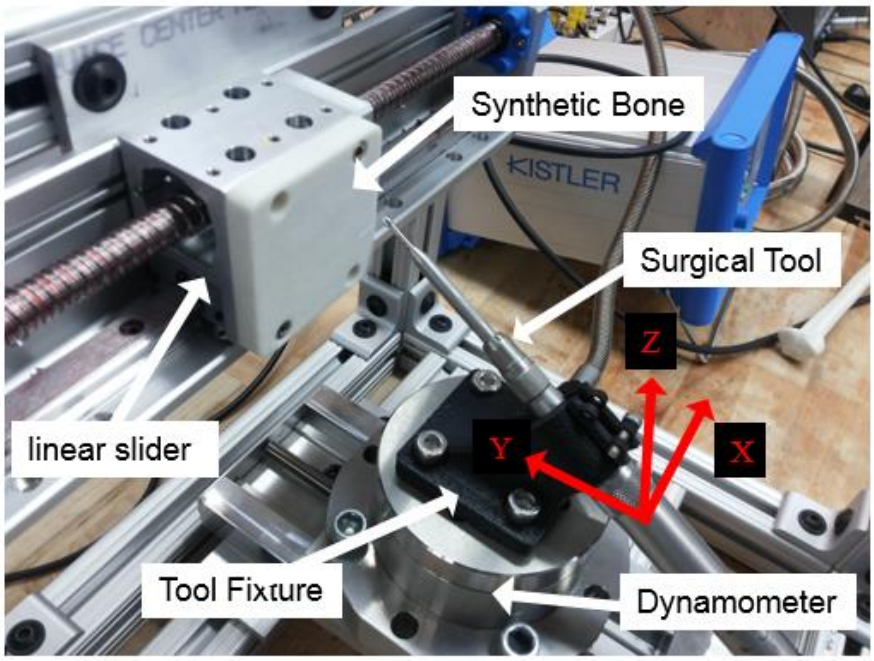

(a)

Figure 3. Photographs shows the experimental setup in (a) Isometric View (b) top view

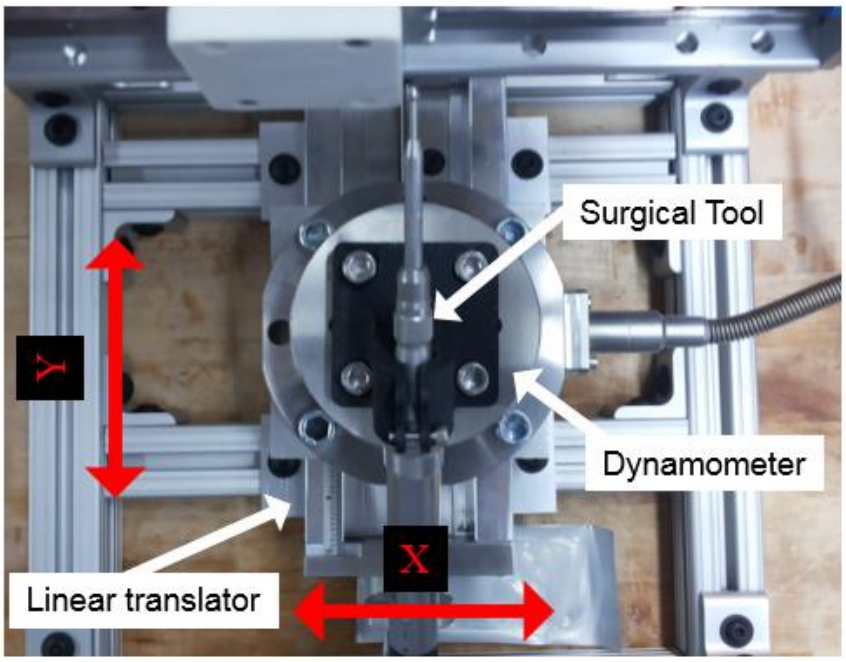

(b)

Figure 3. Continued

2.2 Workpiece and fixture design

Three fixtures are designed for three different cutting angles. The fixtures are shown in the Fig. 4. These fixtures are 3D printed using FDM machines with a high infill to provide robustness. And the workpiece is designed with provision to fit on the linear translator (Fig. 5).

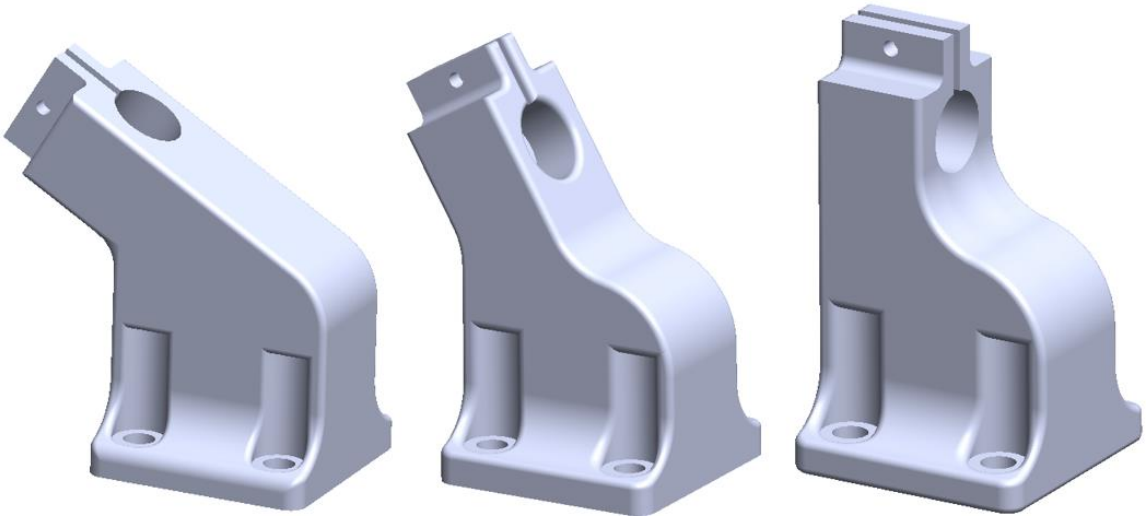

(a) (b) (c)

Figure 4. SolidWorks model of (a) 30 degree fixture, (b) 60 degree fixture, (c) 90 degree fixture

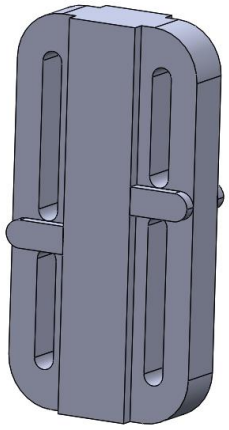

Figure 5. SolidWorks model of workpiece

2.3 Design of experiments

Angle of cutting is the angle between the axis of the drill and the bone surface. Feed rate is the velocity of the tool moving forward relative to the bone surface, which is kept constant at 3mm/s in this case. The depth of cut and spindle speed were kept constant. The depth of cut is taken as 0.5 mm based on the previous studies [21, 22]. The spindle

speed used in the experiments is 60,000 rpm, as it is a common speed used in surgery. The feed rate used in the experiments is 3 mm/sec. Three orientations, parallel cutting, perpendicular cutting and diagonal cutting are considered in our experiments. Fig. 6 shows the three orientations in detail. In parallel cutting (Fig. 6(a)) the axis of the drill and the axis of the groove are in the same vertical plane. In perpendicular cutting (Fig. 6(b)), they are perpendicular to each other. Finally, in diagonal cutting (Fig. 6(c)), the axis of the drill and the axis of the groove are at 45 degree angle to each other. Figure 6 also shows the directions of feed, normal and lateral forces in both parallel and perpendicular cutting. It should be noted that these definitions are based on the burr motion rather than a global Cartesian coordinate system. The experiments were carried out using 30, 60 and 90 degree cutting angles for all three cutting orientations as illustrated in Fig. 7. A total 9 cases (3 orientations and 3 angles) were studied with each one replicated five times. Table 1 shows the parameters used in the design of experiments.

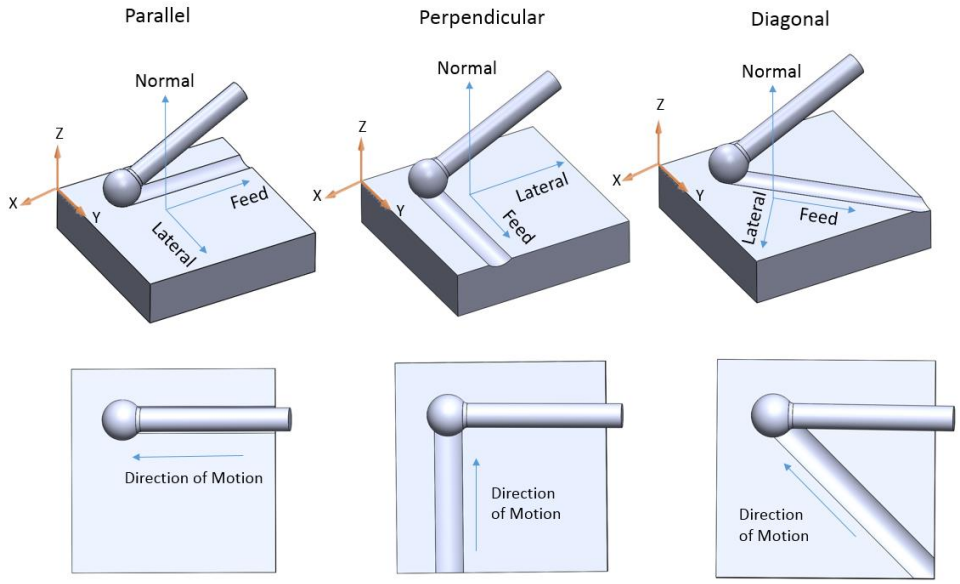

Figure 6. Three burring configurations used in the experimental study are shown in the image. This configuration refers to the feed motion of the burring/cutting tool relative to the workpiece. The tool stem is always in x-z plane: (a) parallel cutting (along *x*-axis); (b) perpendicular cutting (along *y*-axis); (c) diagonal cutting (at a 45-degree angle to *x*-axis and *y*-axis).

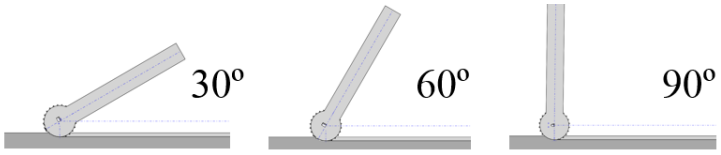

Figure 7. Figure showing the angle of cutting

Tool (Cutting) Angle	30º, 60º, 90º
Feed Motion	Parallel, Perpendicular, Diagonal
Feed Rate (controlled)	3 mm/s
Type of Burr (controlled)	4 mm round abrasive burr
Depth of cut (controlled)	0.5 mm
Spindle speed (controlled)	60,000 rpm

Table 1. Variables used in the design of experiments

2.4 Data processing

The force data is recorded along the x, y and z axis of the dynamometer, as shown in Fig. 3(a) [23]. The force data in Cartesian coordinate was resolved along the axis of the feed, lateral and normal forces in each test. A sample data recorded from the experiments is shown in Fig. 8(a).

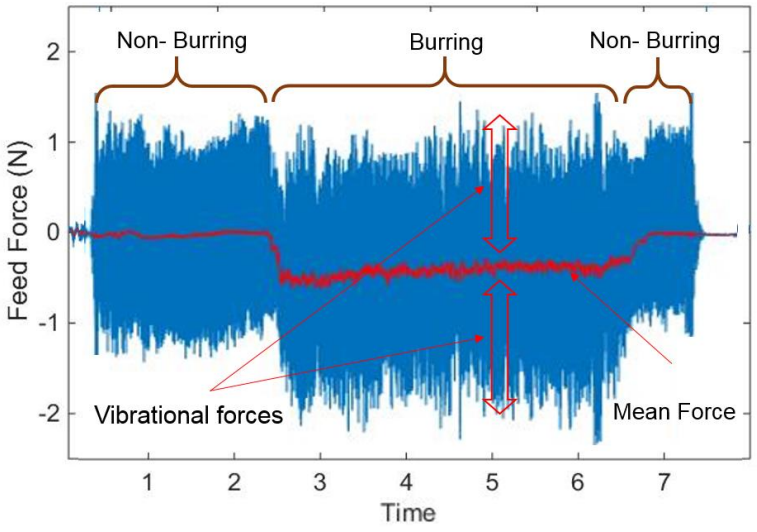

(a)

Figure 8. A sample data showing (a) overall an oscillating force profile and (b) a close-up view that explains the calculation of mean force and vibrational force

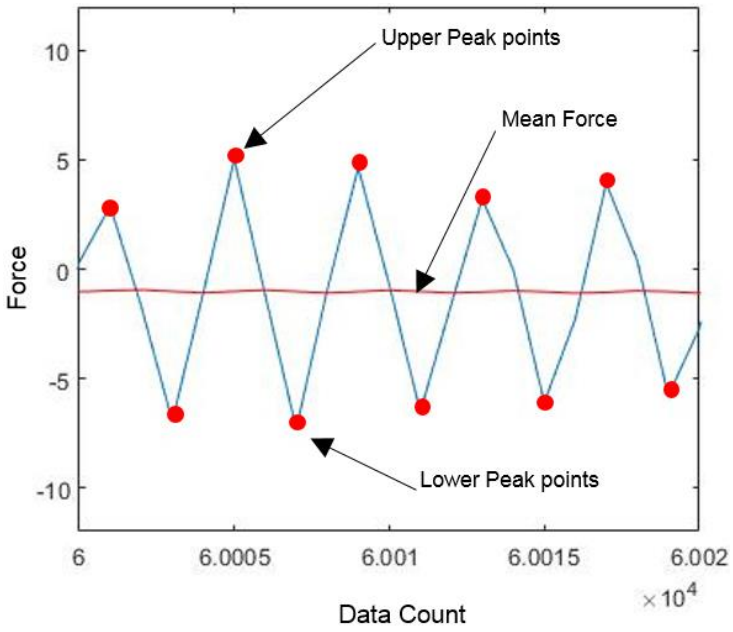

(b)

Figure 8. Continued

As it can be seen in the force profile, mean force (shown in red) is the averaged of the oscillating force profile under a burring process and the vibrational force is the amplitude of the oscillations on either side of the mean force. So, the total force feedback consists of a mean force (or resistive force, $\overrightarrow{F_r}$) and a vibrational force ($\overrightarrow{F_v}$). Also, this force profile can be divided into two regions, "Burring" and "Non-Burring". "Non-Burring" refers to the region on the force profile where the drill is powered (rotating) but not cutting the bone, resulting in an oscillating force profile with mean value close to zero. "Burring" region refers to the region where the drill is cutting the bone material resulting in the shift of the mean value of the force profile.

The value of force will be the average of the mean profile in the "burring" region. The value of the vibrational force will be the amplitude of the force profile as indicated in

the Fig. 8(a). This can be understood more clearly by looking at the figure 8(b). A portion of data from figure 8(a) is magnified and shown in figure 8(b), where a clear oscillating force profile can be observed. The upper and lower peak points of the graph are identified by the red dots. An average value of all the highest point and all the lowest points is computed. Half of the difference between these average values gives the vibrational force (shown in equation-1). These can be automatically computed using a simple algorithm in MATLAB.

Five sets of data were recorded for every set of experimental parameters. The average of these five values for force and vibration are recorded as the final values to that specific set of parameters. However, all the five values of each set are considered when calculating the errors.

2.5 Preliminary results

Preliminary results include findings from the experiments that can be used for developing the mathematical model for computing resistive and vibrational forces. Some of the important findings that had an impact on the development of the model are presented in this section.

2.5.1 Resistive force ($\overrightarrow{F_r}$)

A sample data from the resistive force data recorded for the burring done in parallel direction is shown in the Fig. 9. These resistive forces shown in the graph are recorded in normal, lateral and feed directions for parallel respectively. Even though there is a lot of variation in the data for 90 degree cutting, the increasing force trend with the angle is very clear in case of Fig. 9. The explanation can be derived by understanding a simple concept

in cutting mechanics. The forces recorded in any cutting operation usually reduced with the increase in cutting velocity. This could be due to the reduction of chip thickness with the increase in velocity. But, for a spherical burr, the velocity changes from point to point on the surface of the burr. The points that are closer to the larger diameter of the burr (equator) will have higher velocities compared to the points closer to poles. This can be visualized by the figure 10 and figure 11. However, an average value of the velocity of the points involved in burring can be computed using numerical methods. This average velocity will depend on the cutting angle of the burr and the direction of cutting (parallel, perpendicular & diagonal). The velocities of the points closer to the largest diameter on the burr (equator) are higher than the points closer to the lowest diameters (poles). From the numerical calculations, the average velocity of the surface of the burr involved in burring in parallel direction is found to be lower for 60 degrees (2.93 m/sec) compared to 30 degree (19.63 m/sec) and 90 degrees (14.45 m/sec). The force recorded for 60 degree cutting is higher, which is likely due to its lower average velocity of the points involved in burring process. This confirms the hypothesis that the cutting force is inversely related to the velocity of cutting. Similar explanation can be extended to the other recorded data as well. So, the model to compute the resistive force can use this relation in its formulation.

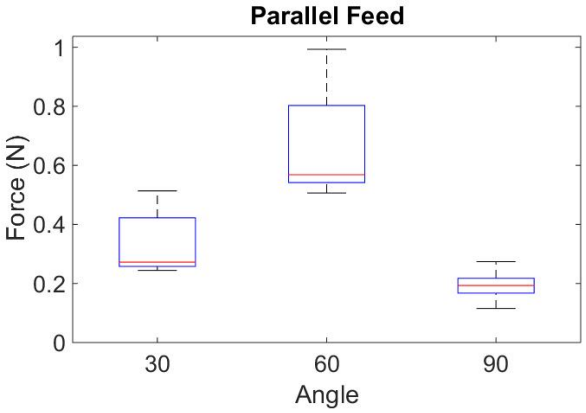

(a)

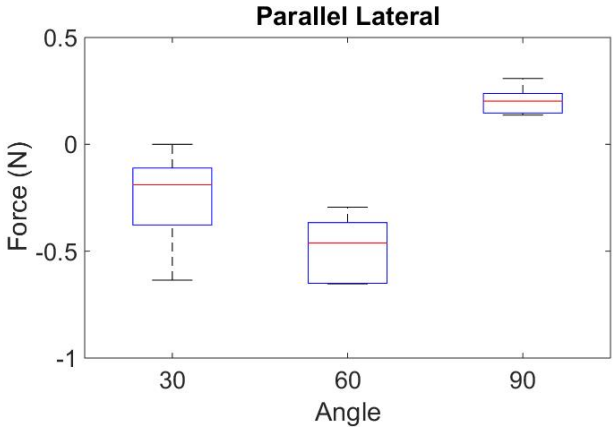

(b)

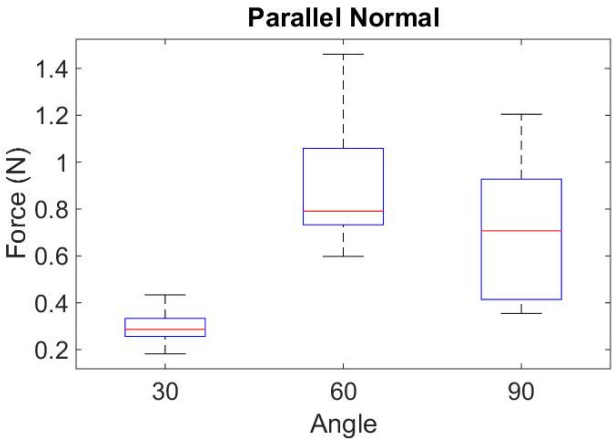

(c)

Figure 9. Resistive force data recorded in parallel cutting (a) Feed (b) Lateral (c) Normal

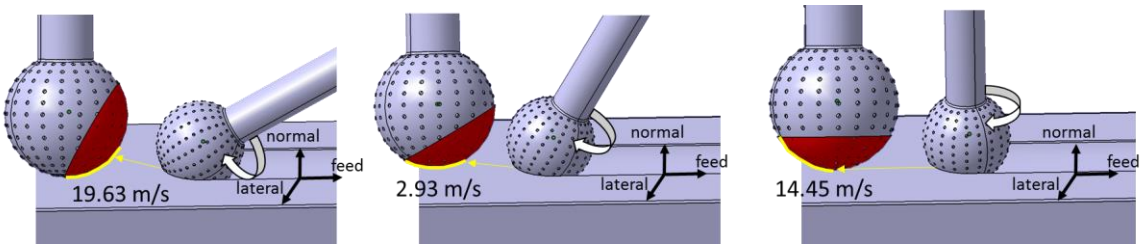

Figure 10. Contact zones and relative motion between burr and workpiece in 30, 60 and 90° cutting angles. The 60° case experiences high force due to low surface velocity in the contact zone

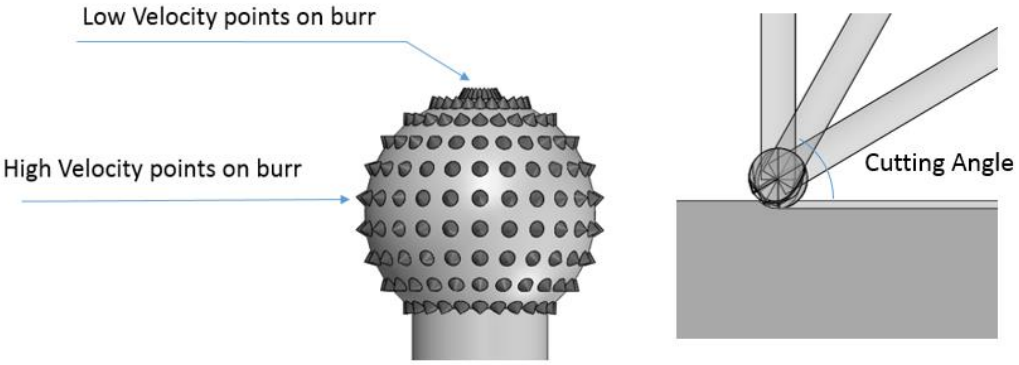

(a) **(b)**

Figure 11. (a) A schematic showing the high and low velocity points on the burr (b) Schematic showing cutting angle.

2.5.2 Vibrational force ($\overrightarrow{F_v}$)

The data recorded in one of the experiments from parallel orientation is shown in Fig. 12(a). This figure shows the force profile and the dominant vibrational frequency in both the "burring" and "non-burring "regions. The force generated from the vibration of the drill originates from the drill's rotating components, whose frequency is dominated by the drill rotation speed. The Fast Fourier Transform (FFT) of the force profiles for burring

and non-burring regions are shown in Fig. 12(b), 12(c). Both graphs show a dominant frequency at 1000Hz, which corresponds to the drill speed at 60,000 RPM. No other major frequencies are recorded in the FFT. This means that the part of the model that calculates the vibrational force in burring can be made to account for only one dominant frequency that is a direct function of the RPM of the drill.

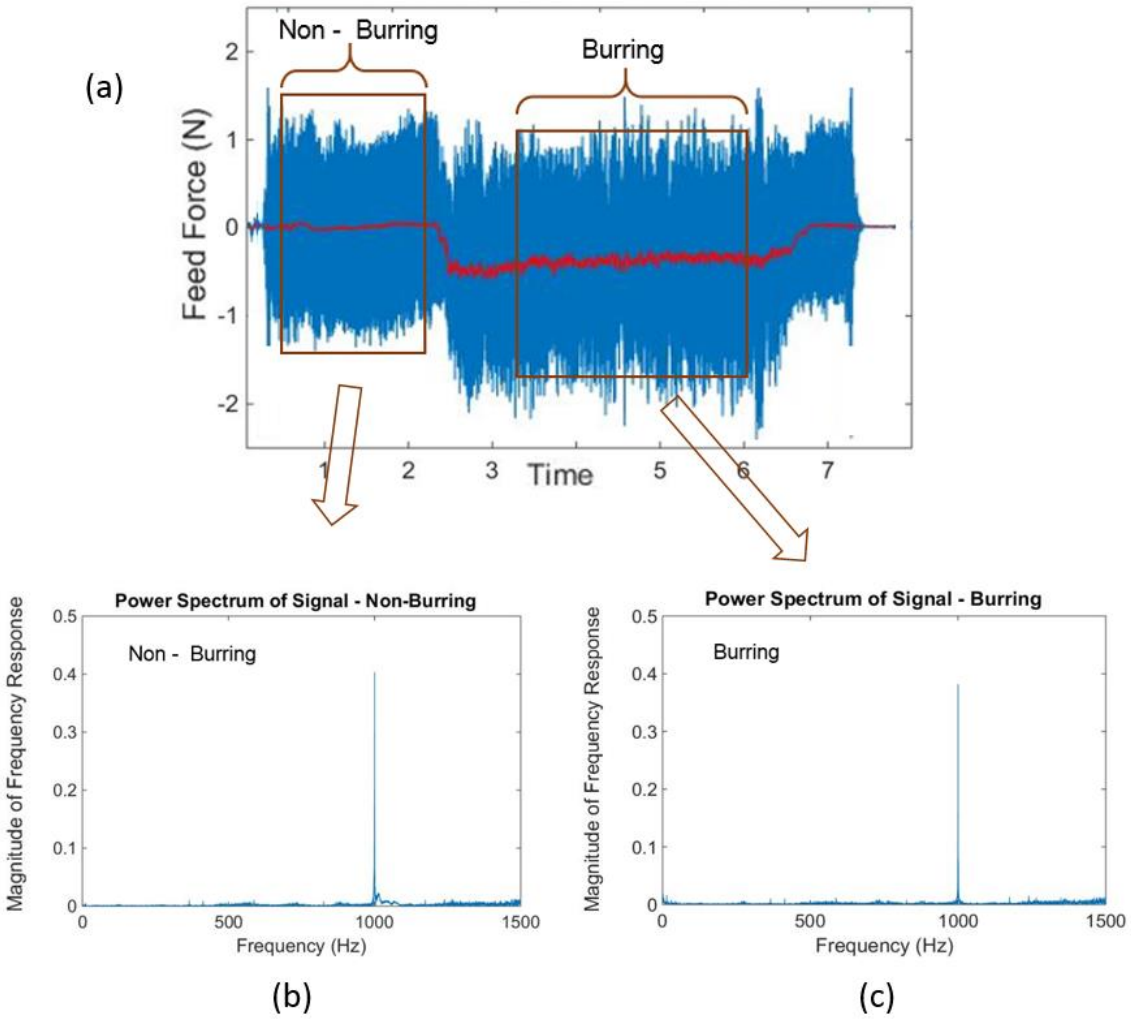

Figure 12. (a) A sample force profile recorded in parallel orientation along feed direction (b) FFT of the force profile for non-burring region and (c) FFT of the force profile for burring regions

In the experiments, the dynamometer records the force profile in all three directions. From these force profiles, resistive force values and vibrational force amplitudes are extracted in all three X, Y, and Z directions for both "burring" and "non-burring" regions. The vibrational force can be computed by subtracting the resistive force from the measured force. Then, the resultant vibrational force ($|\overrightarrow{F_v}|$) can be calculated as a norm of the X, Y, and Z components (i.e., $|\overrightarrow{F_v}|=\sqrt{(F_{vx}{}^2 + F_{vy}{}^2 + F_{vz}{}^2)}$) as shown in Fig. 13. Since the vibrational force is directionless to human perception, this resultant vibrational force can be treated as a single direction force with a given frequency. Following these steps, the averaged resultant vibrational force (F_{av}) can be calculated for all the experiments.

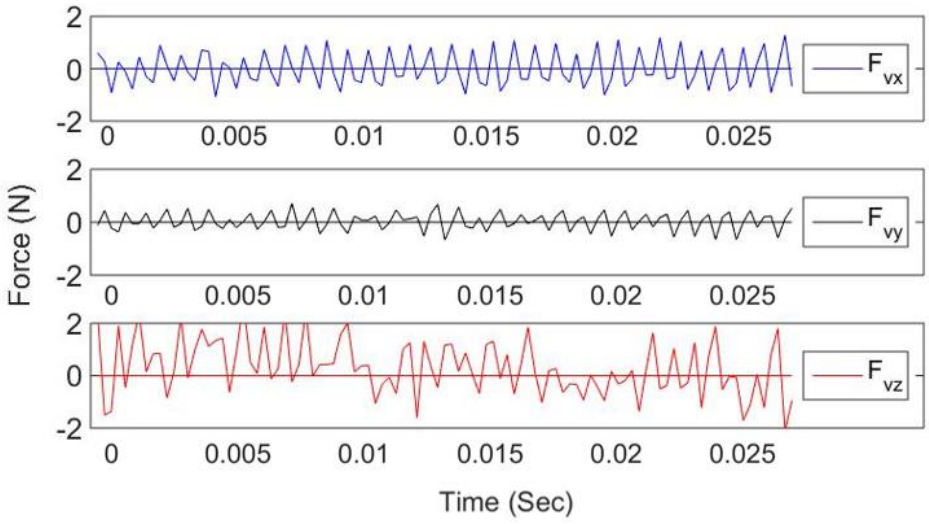

Figure 13. The force profile recorded in X, Y and Z directions

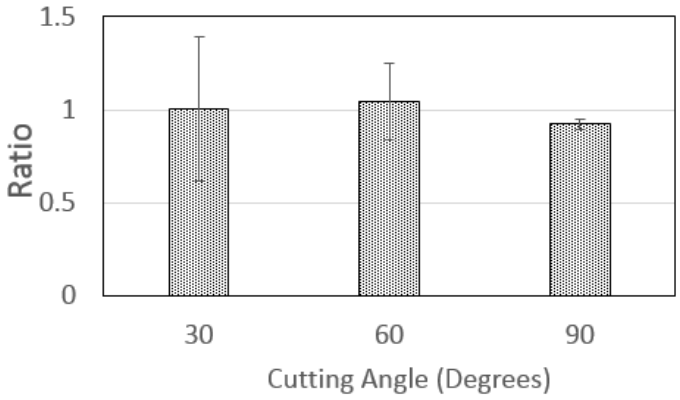

Figure 14. Ratio of vibrational force amplitude recorded in "burring" to "non-burring" condition

Fig. 14 shows the vibrational force data as the ratio of burring to non-burring regions in parallel orientation with three different angles. The ratio is close to one, which implies that there is no significant change in the vibrational force amplitudes between these two regions. This phenomenon is also found in the other two directional settings (perpendicular & diagonal). This results will be explained and implemented into the model in the modeling section (Chapter 3) of this document.

CHAPTER III

MODEL

The surgeon feels two kind of perceivable stimulus when operating with a bone burring drill. One is the resistive force associated with the burring process and the other is the vibration. This can be better understood by looking at the force profile recorded in the bone burring experiments (Fig. 8(a)). In machining, the vibrational force could be a result of insert run-out, chattering, or simply the detailed force profile during a revolution of cut. However, in high-speed bone burring, the vibrational force seems to be from multiple other factors including the motor inside the tool body.

$$\overrightarrow{F} = \overrightarrow{F_r} + \overrightarrow{F_v} \tag{1}$$

In order to understand the force feedback from grinding, it is essential to understand the grinding process and various parameters that effects it. The grinding burr is a spherical tool with diamond abrasives embedded to its surface. There are other types of burrs that are used for removing bone material, however, in this study we are concerned only about the grinding burrs. A schematic of the grinding process is shown in the Fig. 15. Angle of cutting, depth of cut, feed rate, direction of cut and RPM of drill are some of the main parameters that determines the force magnitude during bone burring.

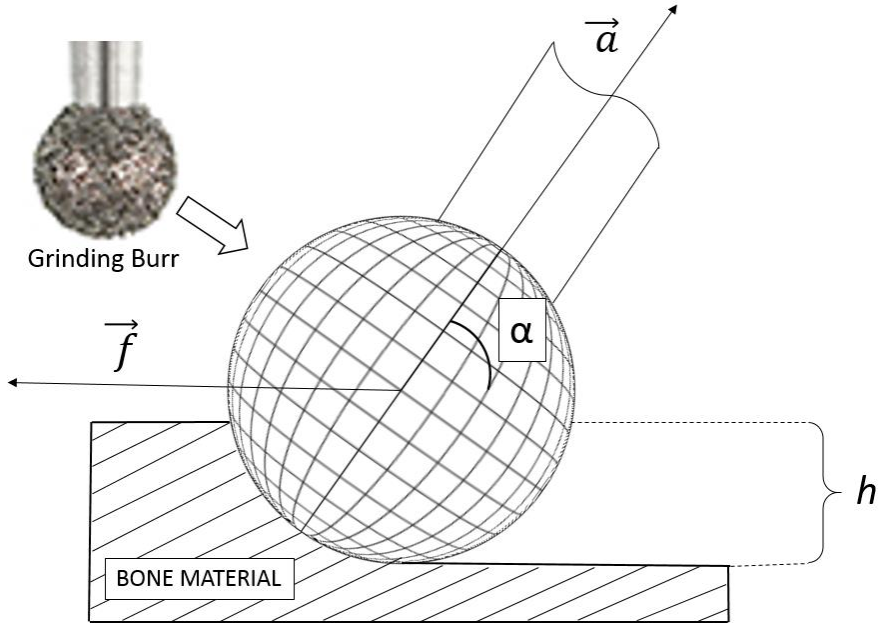

Figure 15. The direction of the axis of the tool ($|\vec{a}|$) and the feed direction ($|\vec{f}\,|$) are shown in the image. 'h' is the depth of cut. 'α' is the angle of cutting

3.1 Resistive Force ($\overrightarrow{F_r}$)

For computing resistive force, the model uses the concept of specific cutting energy, which is the energy expended in removing a unit volume of workpiece material. The central idea of the model is to divide the surface of the burr into several elements and find the force at each element (Fig. 15). The total force on the burr will be the vector summation of the forces on all elements. The force at each element can be calculated using the work done and the distance moved by element (Work = Force × displacement). By calculating the amount of material removed per unit time at each element, we can calculate the amount of energy (work done) expended at each element. The steps involved in the computation of final forces are explained below in detail.

In the force modeling, we calculate the resistive force experienced by the burr in feed, normal and lateral directions (Fig. 6). The first step in the model is to calculate the amount of volume removed per unit time in the direction of each element. This will be same as the volume swept by each element along the direction of the burring (Fig. 16(a)). The curved elements can be approximated to planar quadrilaterals if the number of elements are high enough. Therefore, the volume swept by each element per unit time will be equal to the dot product of area vector ($\overrightarrow{A}$) and feed rate ($\overrightarrow{v_f}$) (2). The amount of energy consumed (work done) to remove this volume will be computed from the specific cutting energy (U_S) value (4).

$$V\ (Volume) = (\overrightarrow{A}\ \cdot\ \overrightarrow{v_f}\ )\ \Delta t \tag{2}$$

$$Work\ done = \ U_S\ \cdot V \tag{3}$$

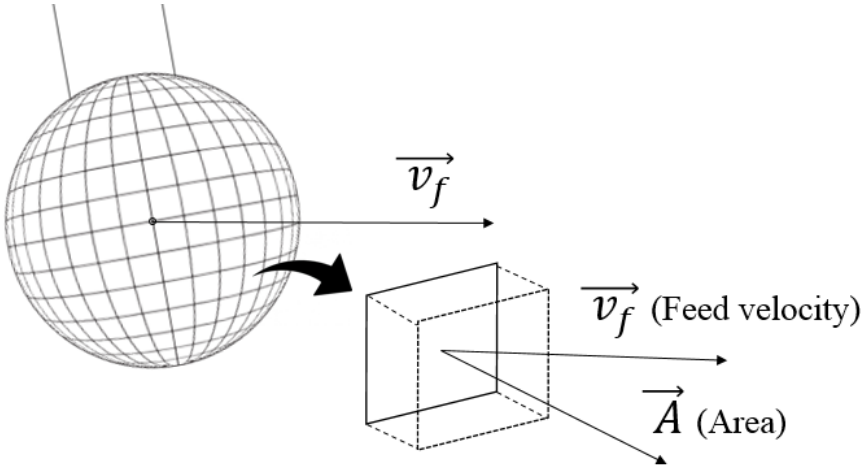

(a)

Figure 16. (a) Image shows a volume swept by the an elemental area on the surface of the burr (b) Normal and Tangential forces on each element

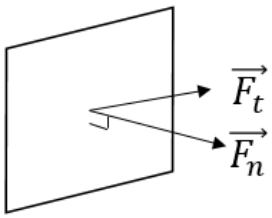

(b)

Figure 16. Continued

The forces on each element during burring can be divided into tangential force $(\overrightarrow{F_t})$and normal force normal force $(\overrightarrow{F_n})$. However, tangential force is the only force responsible for the work done during the burring process. So, the work done will be equal to the work done by this tangential force as shown in (4), where $\overrightarrow{v_t}$ is the tangential velocity of the element. Now, the energy equilibrium relationship can be simplified to (5). Therefore, if the specific cutting energy is known, the tangential force distribution can be determined on the burr surface (since the $\overrightarrow{v_t}$ and V can be computed numerically based on RPM and feedrate).

$$Work\ done = (\overrightarrow{F_t} \,.\, \overrightarrow{v_t}\,)\,\Delta t \qquad \{\overrightarrow{v_t}\,\} \tag{4}$$

$$|\,\overrightarrow{F_t}| \;=\; (\,U_S.\,V)\,/\,(\,|\overrightarrow{v_t}\,|\,.\,\Delta t\,) \qquad \{\text{From (3) and (4)}\} \tag{5}$$

From the theory of grinding, we know that we can approximate normal force as product of tangential force and a constant 'K' (7). It is known form the literature that this ratio of normal force to the tangential force is close to 1.3 and is not constant for all burring conditions. However, in our model we take this ratio as a constant to reduce the complexity of the model. Finally, normal and tangential forces are calculated at each elements and integrated to find the total force on the burr. Since the specific cutting energy is the

property of a material, it is calculated from the experiments. A vector addition of all the normal and tangential forces is conducted and the final resistive force vectors along the feed, normal and lateral directions are computed (7).

$$\overrightarrow{F_n} = \overrightarrow{F_t} . K \tag{6}$$

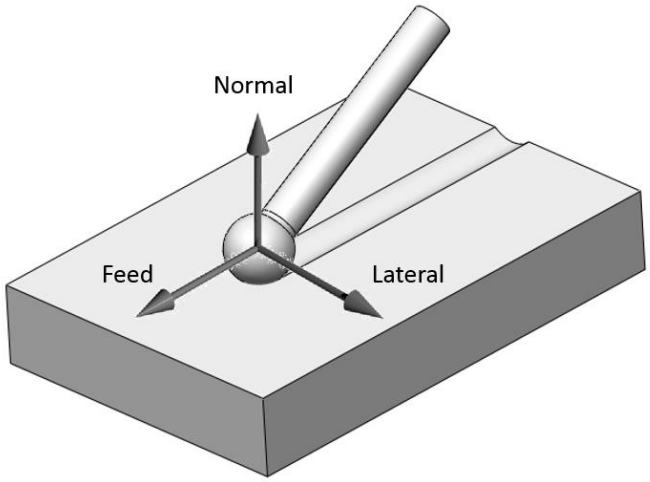

Figure 17. Image showing the directions of feed, lateral and normal forces

$$\begin{aligned} \overrightarrow{F}_{feed} &= \overrightarrow{f} \cdot \sum \overrightarrow{F_n} + \overrightarrow{f} \cdot \sum \overrightarrow{F_t} \\ \overrightarrow{F}_{lateral} &= \overrightarrow{l} \cdot \sum \overrightarrow{F_n} + \overrightarrow{l} \cdot \sum \overrightarrow{F_t} \\ \overrightarrow{F}_{normal} &= \overrightarrow{n} \cdot \sum \overrightarrow{F_n} + \overrightarrow{n} \cdot \sum \overrightarrow{F_t} \\ \overrightarrow{F_r} &= \overrightarrow{F}_{feed} + \overrightarrow{F}_{lateral} + \overrightarrow{F}_{normal} \quad \{\text{Resultant resistive force}\} \end{aligned} \tag{7}$$

3.2 Calculation of Specific Cutting Energy (U_s) Value

Although the specific cutting energy is primarily a material property, it also depends heavily on the type of material removal process and chip thickness (average thickness of the layer of material removed in each revolution) [24]. For example, aluminum has an expected U_s value ranging from 500 GJ/m3 to 9000 GJ/m3 as the chip

thickness decreases from 1 mm to 0.001mm. This can be seen in the graph shown in Fig. 18 [24]. Given the small range of chip thickness difference in high-speed burring with the grinding burr, an averaged Us can be used, which will be determined experimentally. So, the value of this property can be calibrated from the experimental data for the synthetic bone material as well. This means the data recorded from the experiments and the data generated from the model should be compared and the value of the specific cutting energy should be determined.

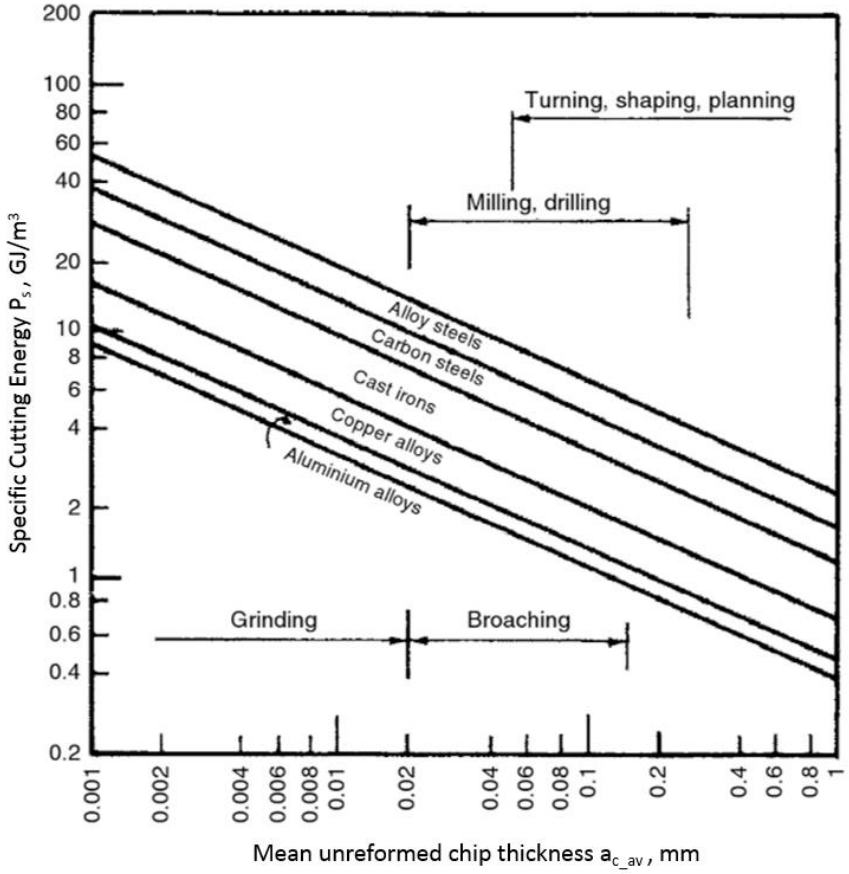

Figure 18. Graph showing the specific cutting energy of different alloys with change in chip thickness. This graph is taken from "Advanced machining process of metallic materials" by Wit Grzesik

The experimental results of the resistive forces measured in parallel and perpendicular burring direction are shown as box plots in figure 19 (diagonal burring not considered). The data is shown for orthogonal feed, normal, and lateral directions. It can be clearly seen that most of these forces are not monotonic functions against orientations. The solid curves are the resistive forces predicted by the model with an optimized specific cutting energy U_s. The determination of U_s is carried out using the MATLAB optimization tool to find the value that best fits the experimental results. So, a range of values for Us were tested in the algorithm, and the value of Us for which the force values from the model are close to the experimental results was chosen as the final value. This value was found to be 805.1 N/mm^2. As aforementioned, this represents the material property and process conditions together, and hence could be different from the specific cutting energy of the material itself. Mathematically, U_s is simply a scaling factor. This means that the consistent trends observed in both experiments and the model verify the ability of the algorithm to predict the force transitions. It is important to note that this optimization is carried out by considering both parallel and perpendicular directions. The data for the diagonal will be used to validate the model.

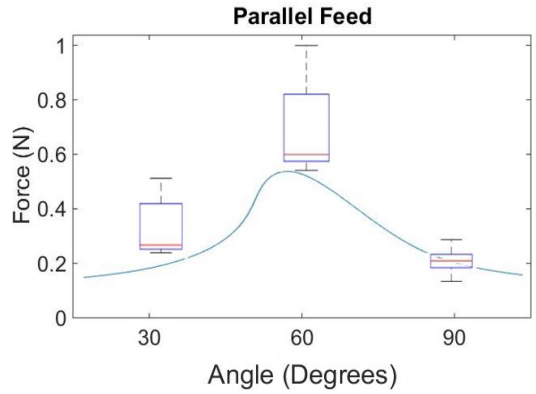

(a)

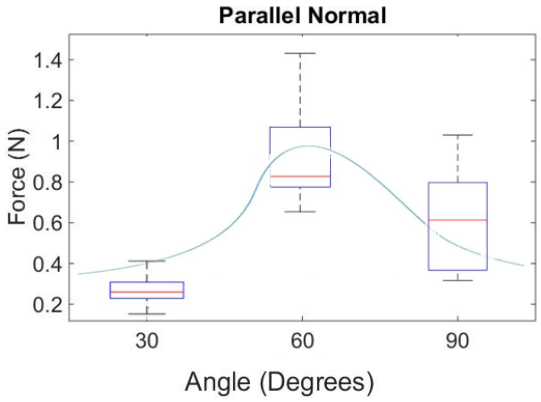

(b)

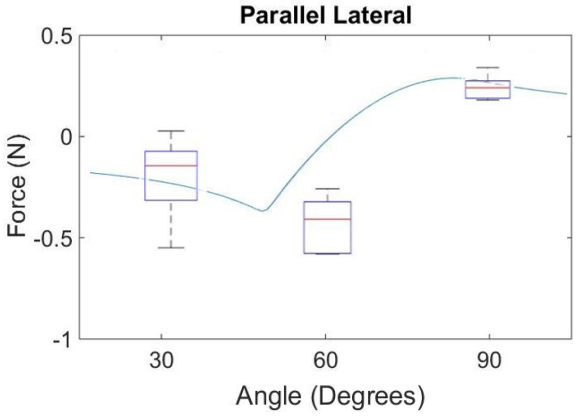

(c)

Figure 19. Box plots and curves generated by the algorithm showing the feed, normal and lateral forces from experiments for 30, 60 and 90 degree cutting angles. (a), (b) and (c) shows the results from parallel cutting and (d), (e) and (f) shows perpendicular cutting.

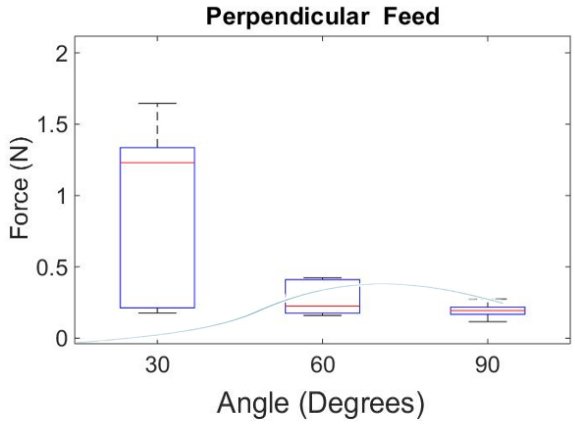

(d)

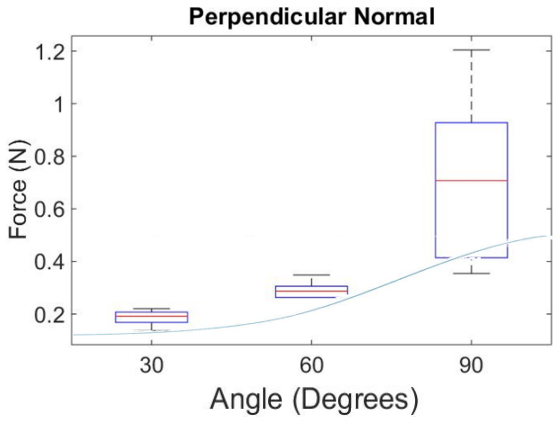

(e)

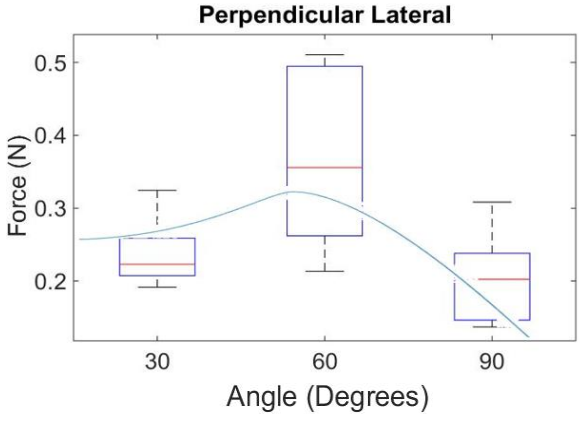

(f)

Figure 19. Continued

3.3 Vibrational Force ($\overrightarrow{\boldsymbol{F_v}}$)

The vibrational force is defined as the amplitude of the oscillating force profile (Fig. 6). The total vibrational force ($\overrightarrow{F_v}$) felt on the burr surface is a combination of vibrational forces generated from bone burring ($\overrightarrow{F_g}$) and the vibrational forces from the drill rotation ($\overrightarrow{F_d}$). The former can be seen as an active cutting force component, which depends on the cutting mechanics and tool conditions. The latter is a background noise generated by the drill motor, structure natural frequency, and boundary conditions. These two terms are generally independent, but the coupled effect could occur when the vibrational frequencies are close to each other, also called chatter. Therefore, mathematically, the resultant vibrational force will be a function of these two individual vibrational forces, as shown in Eq. (8).

$$\overrightarrow{F_v} = f(\overrightarrow{F_g}, \overrightarrow{F_d}) \tag{8}$$

It is well known that the humans cannot perceivably differentiate between the vibrational directions in these ranges of frequencies and amplitudes [15]. This finding could significantly reduce the effort to determine the needed force feedback. The resultant vibration can then be further simplified via a scalar computation using just their amplitudes. The equation (9) shows this simplification.

CHAPTER IV

VALIDATION

To validate the model and the computed U_s (from the parallel cutting and perpinducular cutting) across different feed motions and tool angles, experiments were conducted with the diagonal motions as mentioned in Table 1 and illustrated in Fig. 6. Figure 20 shows the resulting forces in the lateral, feed, and normal directions (as box plots) for diagonal direction compared with the forces predicted by the model (solid, smooth curves). In this diagonal cutting direction, the force model can correctly capture the overall trends and magnitudes, especially the profile transition occurring at about 60° in the lateral case. Variations were seen in certain cases (*e.g.*, 30° in feed, 90° in normal) most likely due to the structural instabilities and dynamic stiffness that could have led to significant vibration. An average magnitude differential of around 0.2 N can be seen between the model and experimental values; however, the trends are generally consistent except the lateral force. This could be due to using a constant U_s. Another possible cause is the assumption of a constant K for model simplicity. This comprise for computational efficiency could have led to loss in accuracy. Nevertheless, while striving to predict a small cutting force magnitude that occurs concurrently with relatively large high-frequency force variations, the model's capability to predict the trends and changes in forces is more useful for the application of haptics calculations.

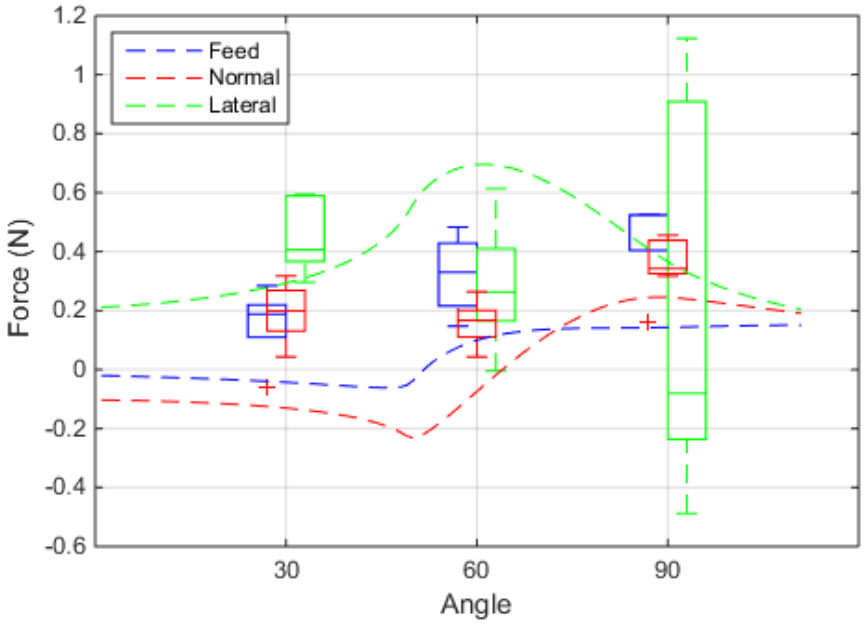

(a)

Figure 20. Comparisons of the algorithm-predicted force curves and experimental data in three cutting angles in diagonal direction.

CHAPTER V

CONCLUSIONS AND FUTURE WORK

The mathematical model developed in this paper predicts the trend in force components under various burring orientations. The model adapted two different techniques to compute resistive and vibration forces. In the case of resistive force, the concept of specific cutting energy was used along with the material removal rate and cutting speed, and the model predicted trends correctly for different orientation. Parameters such as Us, K, and F_d are used as constants in an average sense. Although these can lead to unrealistic predictions in extreme scenarios, it is considered a tradeoff for enabling real-time computation. The model successfully incorporates cutting mechanics to predict forces as a function of orientation, and further simplifies it to gain computational efficiency. The vibrational force was quantified to be a constant based on experimental data. The frequency for this vibrational force was coupled with the RPM of the drill.

This model is likely not accurate if applied to burrs with cutting flutes (cutting burr) instead of burrs with surface embedded with abrasives (grinding burr) due to the fact that cutting edge geometries are not considered in this model. Grinding burrs are unique in the sense of a large amount of homogeneously distributed cutting edges (abrasives), which lead to the development of Eqs. (4)-(6). The homogeneity also results in much smoother bone burring process which explains the lack of relative amplification in vibrational force levels before and during burring (10).

It is also important to note that the spindle speed, feed rate, and depth of cut are

controlled variables in this study. These variables are known to be linearly proportional to the amount of material removed at each element which is in turn proportional to the forces generated at these elements. Since the material removal-to-force relationship is well-developed in machining theory [25], the focus of this work is to further incorporate the effects of burring angle and orientation.

Quantitatively the model has shown an acceptable result, but it has not been proven in a human perception setting yet. Future work includes psychophysical studies to validate the model by artificially generating haptics using this algorithm. The potential refinements of the model include varying K values and applying vibrational force profiles duplicated from the data.

For algorithm implementation, programming based on voxels is possible as they can represent the amount of material removed by each elemental area of the burr (in Eq. (5)). The resistive force feedback to human subject can be provided by a haptic device. However, commercially available haptic devices generally cannot produce high-frequency vibration due to the hardware limitation. Therefore, the vibrational force is likely to be achieved using an additional actuator.

REFERENCES

1. G.J. Wiet, et al., "Virtual temporal bone dissection: an interactive surgical simulator," *Otolaryngology--head and neck surgery : official journal of American Academy of Otolaryngology-Head and Neck Surgery*, vol. 127, no. 1, 2002, pp. 79-83.

2. A. Petersik, et al., "Haptic volume interaction with anatomic models at sub-voxel resolution," *Proc. Haptic Interfaces for Virtual Environment and Teleoperator Systems, 2002. HAPTICS 2002. Proceedings. 10th Symposium on*, 2002, pp. 66-72.

3. D. Wang, et al., "Cutting on triangle mesh: local model-based haptic display for dental preparation surgery simulation," *IEEE Transactions on Visualization and Computer Graphics*, vol. 11, no. 6, 2005, pp. 671-683; DOI 10.1109/TVCG.2005.97.

4. L. Kim and H.S. Park, "Haptic interaction and volume modeling techniques for realistic dental simulation," *The Visual Computer*, vol. 22, no. 2, 2006, pp. 90-98; DOI 10.1007/s00371-006-0369-8.

5. Y. Yoshida, et al., "Development of a multi-layered virtual tooth model for the haptic dental training system," *Dental materials journal*, vol. 30, no. 1, 2011, pp. 1-6.

6. M. Agus, et al., "A multiprocessor decoupled system for the simulation of temporal bone surgery," *Computing and Visualization in Science*, vol. 5, no. 1, 2002, pp. 35-43; DOI 10.1007/s00791-002-0085-5.

7. M. Arbabtafti, et al., "Haptic and visual rendering of virtual bone surgery: A physically realistic voxel-based approach," *Proc. Haptic Audio visual Environments and Games, 2008. HAVE 2008. IEEE International Workshop on*, 2008, pp. 30-35.

8. M. Moghaddam, et al., "A Physically Realistic Voxel-Based Method for Haptic Simulation of Bone Machining," *Haptics: Perception, Devices and Scenarios: 6th International Conference, EuroHaptics 2008 Madrid, Spain, June 10-13, 2008 Proceedings*, M. Ferre, ed., Springer Berlin Heidelberg, 2008, pp. 651-660.

9. M. Arbabtafti, et al., "Physics-Based Haptic Simulation of Bone Machining," *IEEE Transactions on Haptics*, vol. 4, no. 1, 2011, pp. 39-50; DOI 10.1109/TOH.2010.5.

10. Q. Wang, et al., "Impulse-Based Rendering Methods for Haptic Simulation of Bone-Burring," *IEEE Transactions on Haptics*, vol. 5, no. 4, 2012, pp. 344-355; DOI 10.1109/TOH.2011.69.

11. A.M. Okamura, et al., "Reality-based models for vibration feedback in virtual environments," *IEEE/ASME Transactions on Mechatronics*, vol. 6, no. 3, 2001, pp. 245-252; DOI 10.1109/3516.951362.

12. A.M. Okamura, et al., "Vibration feedback models for virtual environments," *Proc. Robotics and Automation, 1998. Proceedings. 1998 IEEE International Conference on*, 1998, pp. 674-679 vol.671.

13. K.J. Kuchenbecker, et al., "Event-based haptics and acceleration matching: portraying and assessing the realism of contact," *Proc. First Joint Eurohaptics Conference and Symposium on Haptic Interfaces for Virtual Environment and Teleoperator Systems. World Haptics Conference*, 2005, pp. 381-387.

14. J.H. Ko and Y. Altintas, "Dynamics and Stability of Plunge Milling Operations," *Journal of Manufacturing Science and Engineering*, vol. 129, no. 1, 2006, pp. 32-40; DOI 10.1115/1.2383070.

15. N. Landin, et al., "Dimensional Reduction of High-Frequency Accelerations for Haptic Rendering," *Haptics: Generating and Perceiving Tangible Sensations: International Conference, EuroHaptics 2010, Amsterdam, July 8-10, 2010. Proceedings*, A. M. L. Kappers, et al., eds., Springer Berlin Heidelberg, 2010, pp. 79-86.

16. H.Z. Tan, et al., "Manual discrimination of compliance using active pinch grasp: The roles of force and work cues," *Perception & psychophysics*, vol. 57, no. 4, 1995, pp. 495-510.

17. S.J. Bolanowski and J.J. Zwislocki, "Intensity and frequency characteristics of pacinian corpuscles. I. Action potentials," *Journal of Neurophysiology*, vol. 51, no. 4, 1984, pp. 793-811.

18. H.Z. Tan, et al., "Human factors for the design of force-reflecting haptic interfaces," *Dynamic Systems and Control*, vol. 55, no. 1, 1994, pp. 353-359.

19. B.L. Tai, et al., "Development of a 3D-printed external ventricular drain placement simulator: technical note," *J Neurosurg*, vol. 123, no. 4, 2015, pp. 1070-1076; DOI 10.3171/2014.12.JNS141867.

20. B.L. Tai, et al., "A physical simulator for endoscopic endonasal drilling techniques: technical note," *J Neurosurg*, vol. 124, no. 3, 2016, pp. 811-816; DOI 10.3171/2015.3.JNS1552.

21. B.L. Tai, et al., "Temperature prediction in high speed bone grinding using motor PWM signal," *Medical Engineering & Physics*, vol. 35, no. 10, 2013, pp. 1545-1549; DOI http://dx.doi.org/10.1016/j.medengphy.2013.05.011.

22. L. Zhang, et al., “Thermal model to investigate the temperature in bone grinding for skull base neurosurgery,” *Medical Engineering & Physics*, vol. 35, no. 10, 2013, pp. 1391-1398; DOI http://dx.doi.org/10.1016/j.medengphy.2013.03.023.

23. Danda, A., Kao, Y.T., Kuttolamadom, M.A., Tai, B.L. (2016) “Characterization of Forces in High-Speed Bone Cutting and Grinding for Haptics Rendering (MSEC2016-8794),” Proceedings of the ASME International Manufacturing Science and Engineering Conference (MSEC 2016), Blacksburg, VA.

24. W. Grzesik, “Advanced Machining Processes of Metallic Materials,” 2008.

25. D.A. Stephenson and J.S. Agapiou, “Metal Cutting Theory and Practice,” 2016.